Motion posture control for power cable maintenance robot in typical operation conditions

Wei Jiang and Meng Huai Peng
Wuhan Textile University, Wuhan, China and Hubei Engineering Research Center for Intelligent Assembly of Industrial Detonators, Wuhan, China
Yu Yan
State Grid of Hunan Electric Power Company Maintenance Company, Changsha, China;
State Grid Laboratory for Live Inspection and Intelligent Operation Technology, Changsha, China and
Hunan Province Key Laboratory for Intelligent Live Operation Technology and Equipment (Robot), Changsha, China
Gongping Wu
Wuhan University, Wuhan, China
An Zhang
Wuhan Textile University, Wuhan, China and Hubei Engineering Research Center for Intelligent Assembly of Industrial Detonators, Wuhan, China
Lianqing Yu
Wuhan Textile University, Wuhan, China, and
Hong Jun Li
Wuhan Textile University, Wuhan, China and Hubei Engineering Research Center for Intelligent Assembly of Industrial Detonators, Wuhan, China

Abstract

Purpose – In the extreme power environment of flexible transmission line, wind load, high voltage and strong electromagnetic interference, the motion performance of the robot manipulator is strongly affected by the extreme environment. Therefore, this study aims to improve the manipulator motion control performance of power cable maintenance robot and effectively reduce the influence of specific operation environment on the robot manipulator motion posture.

Design/methodology/approach – The mathematical model under three typical operation conditions, namely, flexible line, wind load and strong electromagnetic field have been established, correspondingly the mapping relationship between different environment parameters and robot operation conditions are also given. Based on the nonlinear approximation feature of neural network, a back propagation (BP) neural network is adopted to solve the posture control problems. The power cable line sag, robot tile angle caused by wind load and spatial field strength are the input signals of the BP network in the robot motion posture control method.

Findings – Through the training and learning of the BP network, the output control variables are used to compensate the actual robot operation posture. The simulation experiment verifies the effectiveness of the proposed algorithm, and compared with the conventional proportional integral differential (PID) control, the method has high real-time performance and sound stability. Finally, field operation experiments further validate the engineering feasibility of the control method, and at the same time, the proposed control method has the remarkable characteristics of sound universality, adaptability and easy expansion.

Originality/value – A multi-layer control architecture which is suitable for smart grid platform maintenance is proposed and a robot system platform for network operation and maintenance management is constructed. The human–machine–environment coordination and integration mode and intelligent power system management platform can be realized which greatly improves the intelligence of power system management. Mathematical models of the robot under three typical operation conditions of flexible wire wind load and strong electromagnetic field are established and the mapping relationship between different environmental parameters and the robot operation conditions is given. Through the non-linear approximation characteristics of BP network, the control variables of the robot joints can be obtained and the influence of extreme environment on the robot posture can be compensated. The simulation results of MATLAB show that the control algorithm can effectively restrain the influence of uncertain factors such

The current issue and full text archive of this journal is available on Emerald Insight at: **www.emeraldinsight.com/0143-991X.htm**

Industrial Robot: the international journal of robotics research and application
46/5 (2019) 631–641

[DOI 10.1108/IR-01-2019-0015]

Funding: This work was supported by the Hubei Provincial Department of Education Research Project (B2019067) and Wuhan Textile University, Research Project Fund (National Project Cultivation Plan, 2019) and State Grid Hunan Electric Power Company Science and Technology Project.

Received 16 January 2019
Revised 22 February 2019
7 March 2019
Accepted 8 March 2019

as flexible environment, wind load and strong electromagnetic field on the robot posture. It satisfied the design requirements of fast response, high tracking accuracy and good stability of the control system. Field operation tests further verify the engineering practicability of the algorithm.

Keywords Flexible wire, Posture control, Power cable maintenance robot, Flexible conductor, Wind load, Spatial electromagnetic field

Paper type Research paper

1. Introduction

The high-voltage power cable is an important channel for power transmission. Given their overhead suspension, high voltage and current and the harsh geographical environments in which they tend to be deployed, high-voltage power cables are susceptible to such problems as the displacement or rusting of the vibration hammer (Pouliot *et al.*, 2015), pollution flashover of insulators (Ramirez *et al.*, 2014), scattered and broken strands of power cable lines (Singh *et al.*, 2013; Banthia *et al.*, 2014), and tension in the clamp drainage plate or the loosening of bolts of the spacer bar (Wang *et al.*, 2014; Pouliot *et al.*, 2012). Moreover, transmission lines cause changes in the dimensions of line fittings in practice because of differences in construction, maintenance and other factors that lead to the emergence of heterogeneous line fittings. This random uncertainty results in an extreme power cable line environment, presents significant challenges to line maintenance operations, and significantly affects the normal operation of the entire state grid system. To ensure the safety and stable operation of high-voltage transmission lines, it is necessary to carry out regular, as well as irregular maintenance and construction of line fittings and their corresponding operation environment. An effective alternative to manual maintenance is to use mobile robots that can carry operation manipulators and the corresponding end tools; such robots are known as power cable maintenance robots (Buehringer *et al.*, 2010; Montambault *et al.*, 2012). After years of research and development, the operation functions of power cable maintenance robots have gradually diversified, and the equipment of the system platform has improved and matured. However, the problem of operational intelligence has become a major bottleneck because it restricts the application and popularization of power state grid systems, especially in the extreme operating environments of high-voltage power systems involving flexible power cable lines, random wind loads and strong electromagnetic fields. Therefore, it is theoretically and practically important to study posture control of the robot in extreme environments, especially in typical operation conditions of a high-voltage power cable line.

The influence of the operation environment on the robot's posture control is mainly manifested in three aspects. First, the center of gravity of the robot is lower than the reference ground because of its weight and flexible sag in the power cable line, which reduces the length of the robot's operation arm and its corresponding operation end, and causes its posture to deviate from the ideal posture. To eliminate the influence of environment on the robot's posture, error can be compensated for by using the joint stretch motion of the manipulator in real time. The key is to find the intrinsic nonlinear mapping between sag in the conductor and the robot's joint motion compensation value. The oblique parabola model of a flexible power cable line has been developed (Kim *et al.*, 2000; Sun *et al.*, 2016), the corresponding mathematical model has been established, and a qualitative analysis of the geometric characteristics of flexible power cable lines has been conducted. For example, a rigid-flexible dynamic coupling model of a flexible power cable line and a power line inspection robot was established in (Xiao *et al.*, 2005; Xiao *et al.*, 2008; Sun *et al.*, 2010), and the robot's operation mode and power cable line were analyzed. However, these studies failed to reveal the influence of a flexible power cable line on the robot's motion posture, especially from the perspective of its position and posture control. Second, the robot walks on the power cable line, and random wind loads can easily cause the rolling and swaying of its body. This results in a difficulty in focusing the camera and blurs its images, but also affects the location motion control of the object of operation. A large number of invalid photos and videos are thus generated that consume memory, increase the duration of the visual servo control process, and lower location accuracy. Therefore, to eliminate the influence of wind load on the robot's posture, the posture error caused by it can be compensated for by rotating the robot's joint in real time. The key is to identify the internal relationship between the robot's wind angle and the wind load. For example, Hong *et al.* (2016) and Korayem *et al.* (2012) analyzed the influence of wind load on the structural size of a high-voltage inspection robot. The robot's mechanical structure was redesigned and optimized; however, the influence of wind load on its motion posture was not considered. Third, to determine the influence of ultra-high voltage and ultra-strong electromagnetic field on the robot's motion posture, the key is to examine the distribution characteristics of the electromagnetic field around high-voltage lines, and to study the anti-electromagnetic interference control method of the robot's measurement control platform and the software control algorithm. For example, the characteristics of spatial field distribution in a high-voltage electromagnetic environment were analyzed in (Nandhakumar *et al.*, 2013; Wang *et al.*, 2014; Wu *et al.*, 2017; Isaramongkolrak *et al.*, 2014; Lai *et al.*, 2019); however, these studies failed to consider the robot's posture control.

In light of the above, to further improve the stability, real-time performance, location accuracy, and adaptability of the robot in extreme operation environments, this paper proposes control architecture for the multi-modal perception and interaction of a mobile, dual-arm robot in a "man–machine environment." The proposed architecture is intelligent, safe and conducive to man–machine cooperation in extreme power environments. Starting with the examination of a flexible power cable line in the presence of wind load and a strong electromagnetic field, mathematical models of each are established, and mapping relationships between environmental parameters and the robot's operation conditions are given. Because the non-linear approximation characteristics of the BP neural network are similar to those of the process in which the robot's actual posture approaches the ideal posture, the BP network is used for robot posture control, and sag in the power cable line, the robot's wind swing angle and the electromagnetic field are set as input signals to the BP network. Through the training and learning of the network, the output control variables are used to compensate for robot's operation

posture. A simulation verified the effectiveness of the proposed algorithm. Compared with conventional PID control, it can deliver impressive real-time performance and good stability. Finally, field operation tests confirmed the feasibility of the proposed control method. It has the remarkable characteristics of sound universality, adaptability and easy expansion that provide a strong guarantee of effective operation of the robot.

2. Control architecture and motion planning for robot

2.1 Control architecture of smart grid system platform

Through the comprehensive evaluation of the entire operation of the transmission line, we find that its spatial and logical distribution characteristics are important features of maintenance operations. It is a complex system consisting of many sub-processes that acquire the status data of the field power cable line and make decisions regarding maintenance. Therefore, the establishment and implementation of a transmission line maintenance system based on a power cable robot is a solution to distribution problems, and the key is effective control of the robot system. This includes acquiring the robot's operation status, and the coordinated position and attitude control of multiple joints. The control architecture of the power operation robot is shown in Figure 1, where the entire power system consists of different transmission lines. Each conductor is equipped with a maintenance robot and each robot walks on the field power line to maintain power cable faults. Its underlying operational status can be acquired by a signal processing unit and industrial A/D sample cards, and transmitted on a 4 G wireless network to the robot's control base station in the monitoring center of the operation department. The transmission line monitoring center is connected with the monitoring center of the municipal bureau through a public network to share resources and information. At the same time, the monitoring center can send control instructions to the field power cable line through the wireless network to implement the robot's motion control. In this way, the monitoring center can exchange information with the robot in the field environment. This forms an intelligent power grid

Figure 1 Architecture of smart grid platform control

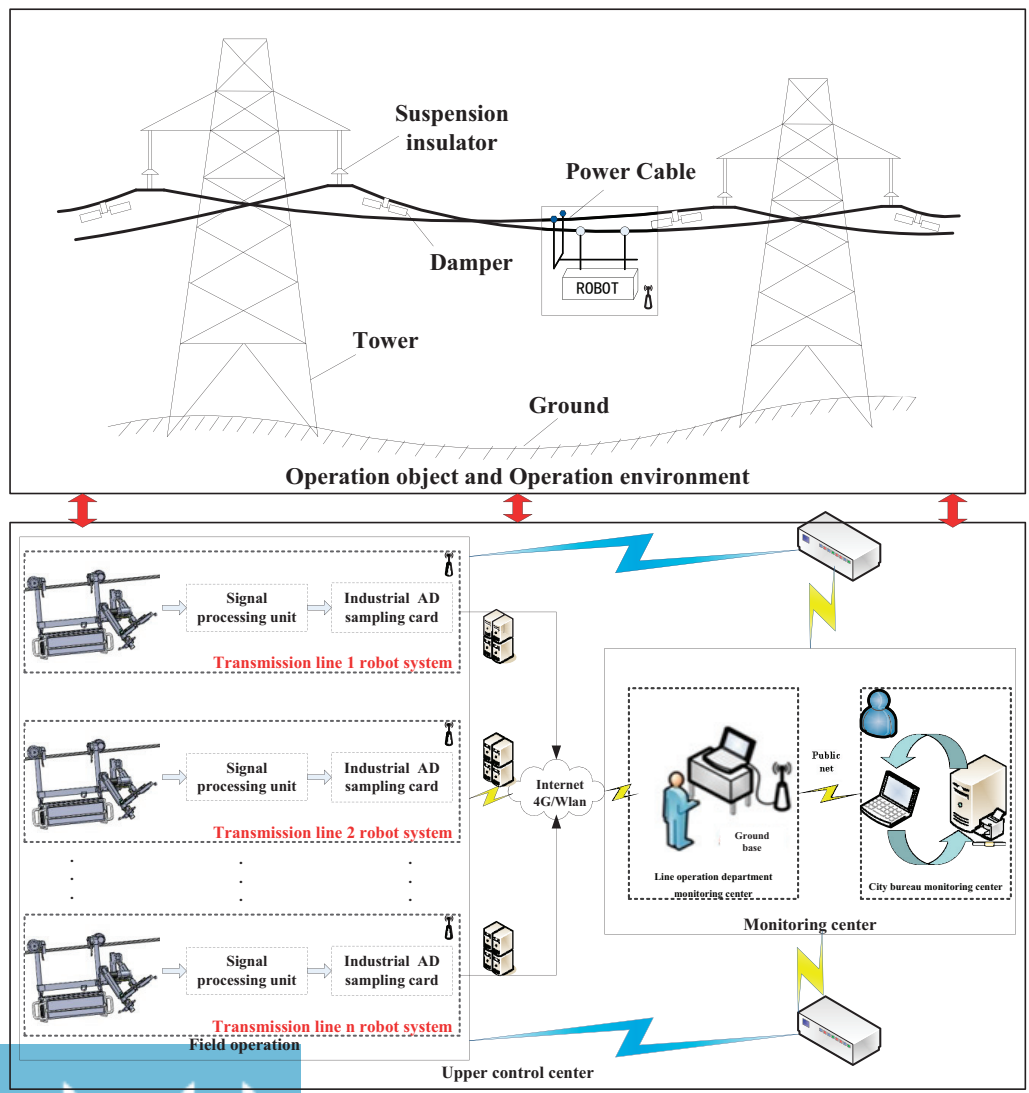

operation and maintenance platform composed of the operation environment of the transmission line, robots, and monitoring centers. In this platform, the function of robot is to assist or replace manual operation, which can significantly reduce operational risk, improve efficiency and implement the intelligent management and operation of the power grid system.

2.2 Motion planning for robot

The robot's operational process can be divided into several steps, and a two-dimensional (2 D) sketch of its motion planning is shown in Figure 2. The robot's double manipulators are first adjusted to the proper posture, and it is lifted up to the transmission line and set there manually. Once manipulator 1 has been adjusted and the bolt head has been aligned and held fixed, manipulator 2 is adjusted and its nut is aligned and held fixed, so that the double-end effector can dock with the nut and tighten (or loosen) it. Following the completion of the operation, the robot moves out of the working area, the manipulators return to their initial postures, and the robot is removed from the line in the same way as it was placed there.

3. Modeling and analysis of power cable operation of robot in typical conditions

3.1 Robot posture model on flexible power cable lines

Figure 3 shows a schematic diagram of the influence of sag in the flexible power cable line on the robot's posture control, wherein Figure 3 (a) is the schematic diagram under ideally rigid conditions where the power cable line has no sag, Figure 3(b) shows the actual, flexible power cable line because of the robot's weight. The flexible conductor has sag, and the robot's body, including the operation end, has dropped by distance $\boldsymbol{H}$. For transmission lines in general, the oblique parabola formula is used to establish the mathematical model of overhead power cable lines using the relevant parameters. The oblique parabolic model of overhead power cable lines is shown in Figure 3 (c), where $\boldsymbol{A}$ and $\boldsymbol{B}$ are the conductor's connection points and components of the conductor's in the adjacent towers, respectively. The origin is connection point $\boldsymbol{A}$, and the oblique parabolic mathematical model is expressed as equation (1):

$$y = \frac{h}{l}x - \frac{\gamma x(l-x)}{2\sigma_0 \cos\beta} \tag{1}$$

where $\boldsymbol{l}$ is horizontal spatial distance (unit $\boldsymbol{m}$) and $\boldsymbol{h}$ is the difference in height between connection points (unit $\boldsymbol{m}$). The difference $\boldsymbol{h}$ is positive when point $\boldsymbol{B}$ is higher than point $\boldsymbol{A}$. β is the angle between a straight line and the horizontal passing through two connection points, and is positive when $\boldsymbol{B}$ is lower than $\boldsymbol{A}$. γ is the specific line load (unit $\boldsymbol{N/m \cdot mm^2}$) and σ_0 is the horizontal stress or stress at the lowest point (unit $\boldsymbol{N/mm^2}$). The coordinates of suspension $\boldsymbol{A}(x_A, y_A)$ are (0, 0), those of suspension $\boldsymbol{B}(x_B, y_B)$ are (l, h) as shown in Figure 3 (c), and the slope $\boldsymbol{y'}$ of point $\boldsymbol{C}$ (x, y) on the conductor between sections $\boldsymbol{A}$ and $\boldsymbol{B}$ is As in equation (2):

$$y' = \tan\theta_o = \frac{h}{l} - \frac{\gamma l - 2\gamma x}{2\sigma_0 \cos\beta} = \frac{h}{l} - \frac{\gamma l}{2\sigma_0 \cos\beta} + \frac{\gamma x}{\sigma_0 \cos\beta} \tag{2}$$

Figure 2 Motion planning for robot

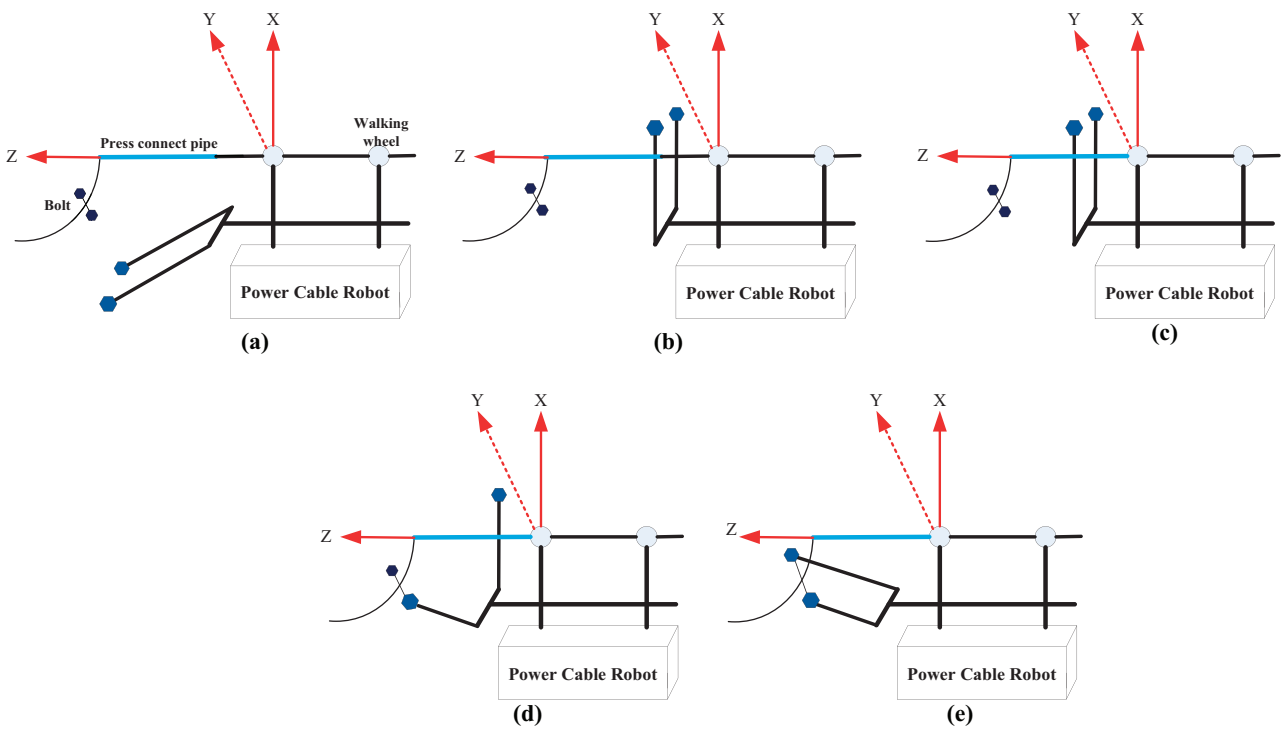

Notes: (a) Double arm initial posture; (b) double arm operation posture; (c) location press connect pipe; (d) location bolt head; (e) bolt tightening

Figure 3 Influence of flexible power cable line on the robot's posture

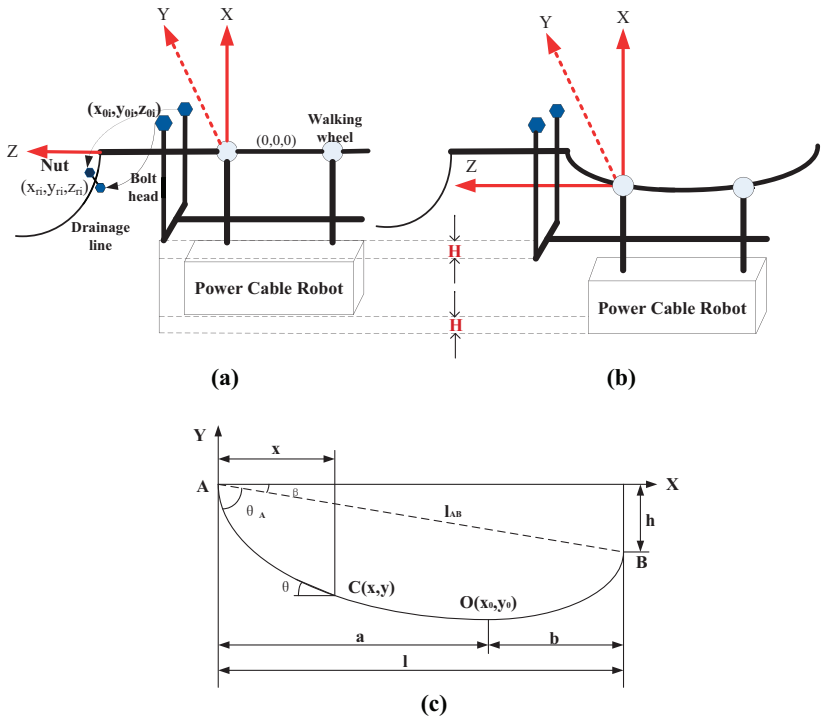

Notes: (a) Ideal rigid conductor; (b) actual flexible conductor; (c) oblique parabolic model of flexible conductor

In equation (2), $\theta_0$is the gradient of any point C on the power cable line between section AB. The line length L of point C from origin A is expressed as equation (3), and can be obtained through the integral of the arc length differential:

$$L = \int_0^x \sqrt{1 + \left(\frac{dy}{dx}\right)^2}\, dx = \frac{1}{\cos\beta_0}\int_0^x \sqrt{1 + \left[\left(\frac{\gamma(l-2x)}{2\sigma_0}\right)^2 - \frac{\gamma(l-2x)}{\sigma_0}\sin\beta\right]}\, dx \tag{3}$$

The equation (3) can be simplified to obtain equation (4):

$$L = -\frac{\gamma^2\cos\beta}{6\sigma_0^2}x^3 + \left(\frac{1}{2\sigma_0\cos\beta} - \frac{\gamma^2 l\cos\beta}{4\sigma_0^2}\right)x^2 + \left(\frac{1}{\cos\beta} - \frac{\gamma l\sin\beta}{2\sigma_0\cos\beta} + \frac{\gamma^2 l^2\cos\beta}{8\sigma_0^2}\right)x \tag{4}$$

where L can be obtained through the speed integration of encoder information with time, and the intercept method can be used to solve for x. The principle of root selection is the positive root less than L and x can be obtained by the abscissa method. Point $O(x_O, y_O)$ is the lowest point on the line, and its slope y' is zero. The equation (5) can thus be obtained from equation (2):

$$x_O = \frac{l}{2} - \frac{h\sigma_0\cos\beta}{l\gamma} \tag{5}$$

By substituting x_0 into the oblique parabolic equation, the corresponding y_0 can be obtained. The approximate sag length is shown in equation (6). Because the robot can be abstracted as an ideal particle relative to the long transmission line, the descent of its body caused by the flexible power cable line can be approximated as equation (6):

$$H = \frac{h}{l}\left(\frac{l}{2} - \frac{h\sigma_0\cos\beta}{l\gamma}\right) - \frac{\gamma\frac{l}{2} - \frac{h\sigma_0\cos\beta}{l\gamma}\left(l - \frac{l}{2} - \frac{h\sigma_0\cos\beta}{l\gamma}\right)}{2\sigma_0\cos\beta} \tag{6}$$

3.2 Rolling model of robot under wind load

Figure 4 shows a diagram of the robot rolling under the action of wind load, and Figure 4 (a) shows the robot without wind load under ideal conditions, it has no tilt. Figure 4 (b) shows that under wind load, the robot's body including the operation manipulator has a roll angle ϑ. When studying the influence of wind load on the robot's motion control, it is assumed that the power cable line is rigid and has little effect on the shape of the suspension. The overhead power cable line between suspension points can be approximated to a flexible chain articulated everywhere. The model of the influence of wind load on the structural parameters of the robot is established as shown in Figure 4 (c). Wind loads on the robot can be simplified into three directions: lateral wind force F_x, lift force F_y, and wind force F_z in the direction of the

Figure 4 The effect of wind load on the robot's posture

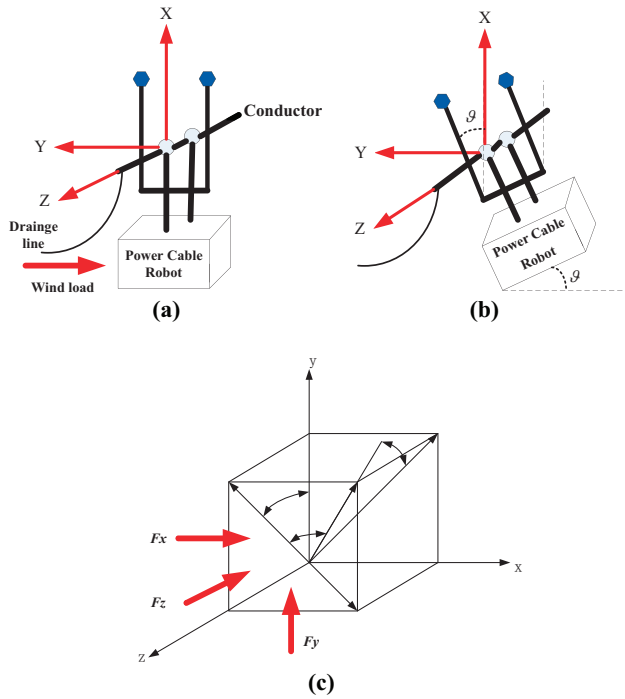

Notes: (a) Ideal windless load; (b) actual wind load; (c) robot wind load force diagram

robot's motion. $\boldsymbol{F}_z$ and the speed of the robot are along the same or in opposite directions, which affects the robot's walking speed. The lateral wind force $\boldsymbol{F}_x$ and lift force $\boldsymbol{F}_y$ mainly affect the robot in left–right lateral swing and up–down vibration along the axis of the power cable line, and show a certain periodicity. According to quasi-static theory, the lateral wind force $\boldsymbol{F}_x$ can be obtained as shown in equation (7), wherein $\boldsymbol{\rho}$ is air density, $\boldsymbol{\alpha}$ is the non-uniform coefficient of wind speed, $\boldsymbol{K}$ is the aerodynamic coefficient, $\boldsymbol{K_h}$ is coefficient of high-altitude wind speed, $\boldsymbol{A}$ is the equivalent area of projection on the windward side, $\boldsymbol{v}$ is wind speed, and φ is the angle between wind load and the windward side. Therefore, the robot's wind swing angle ϑ can be obtained as equation (7):

$$F_x = \frac{1}{2}\rho\alpha K K_h A v^2 \cos\varphi \tag{7}$$

$$\vartheta = \arctan\frac{F_x}{mg} \tag{8}$$

3.3 Circuit model of robot in strong electromagnetic environment

By referring to the technical specifications of the environmental impact assessment of electromagnetic radiation for a 500 kV UHV transmission project, the spatial electric field intensity at any point can be calculated through the equivalent charge method. The charge in the transmission line is line charge, and the radius of the conductor is far smaller than the height of the tower. Therefore, it can be simplified as the equivalent charge at the center of the conductor that can be calculated by using equation (9):

$$\begin{bmatrix} U_1 \\ U_2 \\ U_3 \\ \cdots \\ U_N \end{bmatrix} = \begin{bmatrix} \chi_{11} & \chi_{12} & \cdots & \chi_{1N} \\ \chi_{21} & \chi_{22} & \cdots & \chi_{2N} \\ \cdots & \cdots & \cdots & \cdots \\ \chi_{N1} & \chi_{N2} & \cdots & \chi_{NN} \end{bmatrix} \begin{bmatrix} Q_1 \\ Q_2 \\ Q_3 \\ \cdots \\ Q_N \end{bmatrix} \tag{9}$$

In the above, U is the ground voltage matrix of the transmission line, Q is the equivalent charge matrix of each conductor, χ is a square matrix composed of the potential coefficients of transmission lines, and N is the number of conductors. When the equivalent charge of a unit conductor is obtained, the spatial electric field intensity at any point along the x and y directions is as in equation (10):

$$\begin{cases} E_x = \dfrac{\sum_{i=1}^{m} Q_i \left[\dfrac{x - x_i}{L_i^2} - \dfrac{x - x_i}{(L_i^*)^2}\right]}{2\pi\xi_0} \\ E_y = \dfrac{\sum_{i=1}^{m} Q_i \left[\dfrac{y - y_i}{L_i^2} - \dfrac{y - y_i}{(L_i^*)^2}\right]}{2\pi\xi_0} \end{cases} \tag{10}$$

In equation (10), x_i and y_i are coordinates of conductor i ($i = 1, 2...m$), m is the number of conductors, L_i is the distance between conductor i and the calculated point, and Li^* is the distance between the mirror image of conductor i and the calculated point. According to the superposition principle, the synthetic field strength at points (x, y) is $E = \sqrt{E_x{}^2 + E_y{}^2}$. Therefore, given $110\,kV$ voltage grade transmission lines, according to phase sequence A-B-C-A^*-B^*-C^*, the distribution of electric field intensity $1.5\,m$ above ground and 0–$35\,m$ from the center of the line can be calculated and is shown in Table I.

Table I shows that the smaller the distance to the center of the conductor, the higher the electric field intensity. The highest electric field intensity was $820\,\boldsymbol{V \cdot m^{-1}}$ $1.5\,\boldsymbol{m}$ above ground. When the robot was near the conductor, the electric field intensity was much greater than this value. Similarly, when the robot is hoisted online through the insulated rope, because the rope itself has better insulation, leaked current through the robot is smaller. As the robot approaches the live conductors, electromagnetic induction become stronger, and the local electric field strength between robot and object of operation increases. When the distance between the robot and the conductor is small enough, the air is in free state, and the robot and conductors discharge through the air to generate arcs accompanied by clicking sounds. When the robot's wheels are

Table I Spatial distribution of magnetic field around conductor

The distance to center conductor (*m*)	Electric field strength (*V/m*)
0	820
5	793
10	568
15	317
20	144
25	45
30	20
35	12

fully aligned or the operation end touches the object of operation, negative and positive charges can be neutralized, and both are at the same potential. It is clear that the equipotential process between the robot and the conductor produces a large transient capacitive discharge current. Therefore, the equivalent circuit diagram of the robot entering and exiting the electric field can be obtained as shown in Figure 5. U_C is the potential difference between the robot and the object of operation, C is the capacitance between them, and R is the resistance of the robot's body. When the robot is close to the live conductor along the insulator, the air ionizes and forms a discharge circuit. The instantaneous discharge is equivalent to that of the switch k, and the initial value of the impulse current is $I_s = U_C/R$.

According to the above analysis, when the robot enters or exits the electric field, it withstands the transient impulse current. Therefore, from the perspective of reducing the number of charges and discharges between the robot and the object of operation, equipotential wheels are installed on the robot's platform and connected by compression springs, which can prevent the wheels from slipping or going temporarily offline as it climbs the power cable line. The equipotential wheels maintain sound contact with the conductor as well as balance between the robot and the transmission line. To prevent the electromagnetic field around the conductor from interfering with the robot's hardware control system, electromagnetic interference protection measures are used in the design and development of its control hardware circuit board, control hardware integration, assembly and mechanical structure. The strong ground (GNDP) and weak ground (GNDD) in the control system are separated. The magnet connection between GNDP and GNDD can effectively reduce interference between strong signal fluctuation and the weak signal. GNDP and GNDD are connected through the magnet and cabinet (Eearth_GND) as shown in Figure 6.

In the integrated assembly of the hardware control system, shielding tape is used to wrap the transmission cables of the motors and sensors, and is connected with the robot's cabinet so that the surface of the transmission cable is connected to the cabinet's ground (Eearth_GND). In the mechanical structure, to

Figure 5 The equivalent circuit diagram of robot entering or leaving the electric field

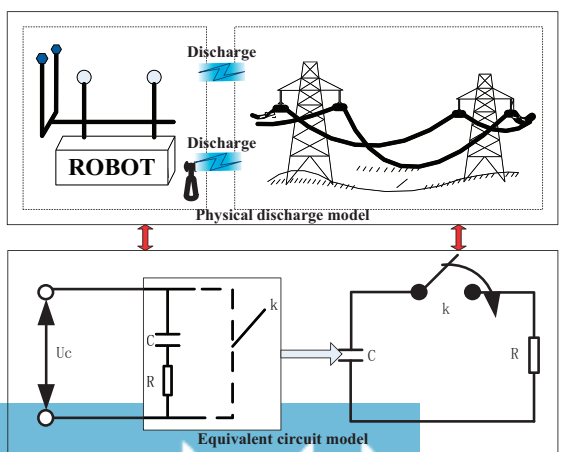

Figure 6 Electromagnetic interference protection for robot's hardware control system

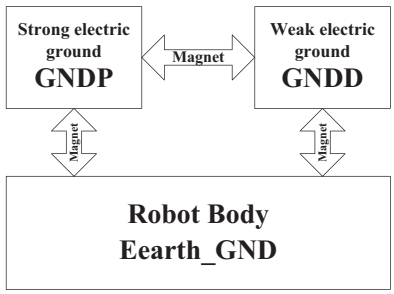

reduce the robot's tip discharge in a strong electromagnetic field, the chamfering process is adopted at the tip. To reduce the influence of discharge at the edge of the control box in the hardware control system, a voltage equalization ring is installed on both sides of the control box. At the front walking wheel, the equipotential wheel is designed to maintain sound contact between the robot's cabinet and the conductor, which minimizes potential difference. External current cannot penetrate the robot system, and this reduces interference with the robot's hardware control system due to the strong electromagnetic field.

3.4 Unifying model under different operation conditions

The above analysis shows that the degree of influence of the flexible power cable, wind load, and strong electromagnetic field on the robot's motion control can be characterized by the flexible conductor sag H, the robot's tilt angle ϑ and the operational spatial electric field intensity E. These disturbances and uncertainties can be compensated for by robot motion control. Therefore, regarding H, ϑ and E, different values can be used to describe different operation conditions, and mapping models of eight conditions and environmental parameters can be obtained as shown in Table II.

4. Design of robot's motion controller in typical conditions

4.1 Basic structure and principle of controller

To achieve precise posture motion control of the robot, real-time posture motion compensation is needed to mitigate the influence of uncertainty and disturbance in specific environments. Neural networks have strong nonlinear approximation characteristics (Cuong *et al.*, 2015; Liu *et al.*, 2016). The process of neural network training is very similar to that of approaching the ideal posture. Therefore, this paper implemented a mapping relationship between the posture compensation values of the robot's joint control variables and its environmental parameters through the BP network in the operation environment. The standard three-layer network structure is adopted in the control system. Because key factors in a given environment are flexible conductors, wind loads, and a strong electromagnetic field, the input to the BP network can be chosen as three nodes. Because the joint output variable value O is used to control the motion of the dual arms, and given that there are seven joints of the dual arms with one extra walking joint, the output of the BP network is selected as eight nodes. To ensure a high speed of network training and the accuracy of the output, the neural network

Table II Mapping model of robot's operation conditions and environmental parameters

Type	Environmental parameters	Robot operation conditions
Case 1	$H=0, \vartheta=0, E=0$	Not flexible, no wind, no electromagnetic field
Case 2	$H=0, \vartheta=0, E>0$	Not flexible, no wind, electromagnetic field
Case 3	$H=0, \vartheta>0, E=0$	Not flexible, wind load, no electromagnetic field
Case 4	$H=0, \vartheta>0, E>0$	Not flexible, wind load, electromagnetic field
Case 5	$H>0, \vartheta=0, E=0$	Flexible, no wind, no electromagnetic field
Case 6	$H>0, \vartheta=0, E>0$	Flexible, no wind, electromagnetic field
Case 7	$H>0, \vartheta>0, E=0$	Flexible, wind load, no electromagnetic field
Case 8	$H>0, \vartheta>0, E>0$	Flexible, wind load, electromagnetic field

controller contained 15 hidden layer nodes. Its output was used to control the motion of the robot's joints to obtain a new robot posture. The new sag, wind tilt angle, and spatial field strength can be obtained through a transmitter device, such as an inclination sensor and a magnetic field sensor, and control deviation can be obtained by comparing the ideal value with the input to the neural network controller. The entire closed-loop control process can be completed by multi-round dynamic adjustment until the error satisfies the control requirements. The basic structure of the closed-loop control system of the neural network is shown in Figure 7.

4.2 Design of BP network control algorithm

In the closed-loop control system in Figure 7, once its structure has been determined, the network needs to be trained and learned by dynamically adjusting the weights of each layer. The function *Random ()* is first used to initialize the weights of the hidden layers and the output layer of the BP network. Input learning samples from N groups are used to calculate the input and output of each layer. The total output error E_A of all samples in a given iteration can be calculated according to equation (11). d_p is the expected output when the *p-th* sample is entered, y_p is the corresponding actual output, and N is the total number of samples. The weights of each layer are modified according to equations (12), (13), (14) and (15) (i is the number of nodes of the input layer, j is the number of nodes of the hidden layer, and k is the number of nodes of the input layer). y_p and E_A can be calculated according to the adjusted weights. If the system total network error $E_A<\varepsilon$ or the maximum number of learning iterations are reached, the learning process is terminated; otherwise, a new round of learning commences.

$$E_A = \sum_{p=1}^{N} E_p = \frac{1}{2}\sum_{p=1}^{N}\left(d_p - y_p\right)^2 \tag{11}$$

$$\Delta\omega_{ij} = -\eta\frac{\partial E_A}{\partial\omega_{ij}}, \Delta\omega_{jk} = -\eta\frac{\partial E_A}{\partial\omega_{jk}} \tag{12}$$

$$\begin{aligned}\frac{\partial E_A}{\partial\omega_{ij}} &= \sum_{p=1}^{N}\frac{\partial E_p}{\partial\omega_{ij}} = \sum_{p=1}^{N}\sum_{j=1}^{n}\frac{\partial E_p}{\partial y_p}\frac{\partial y_p}{\partial u_p^*}\frac{\partial u_p^*}{\partial x_{jp}^*}\frac{\partial x_{jp}^*}{\partial u_{jp}}\frac{\partial u_{jp}}{\partial\omega_{ij}} \\ &= -\sum_{p=1}^{N}\sum_{j=1}^{n}(d_p - y_p)y_p(1-y_p)\omega_{jk}x_{jp}^*\left(1-x_{jp}^*\right)x_p\end{aligned} \tag{13}$$

$$\begin{aligned}\frac{\partial E_A}{\partial\omega_{jk}} &= \sum_{p=1}^{N}\frac{\partial E_p}{\partial\omega_{jk}} = \sum_{p=1}^{N}\frac{\partial E_p}{\partial y_p}\frac{\partial y_p}{\partial u_p^*}\frac{\partial u_p^*}{\partial\omega_{jk}} \\ &= -\sum_{p=1}^{N}(d_p - y_p)y_p(1-y_p)x_{jp}^*\end{aligned} \tag{14}$$

$$\omega_{ij}^{+} = \lambda\omega_{ij} + \xi\Delta\omega_{ij}, \omega_{jk}^{+} = \lambda\omega_{jk} + \xi\Delta\omega_{jk} \tag{15}$$

When adjusting the connection weights of the BP network, to improve the speed of convergence of the proposed algorithm, the momentum term of the previous memory moment weights is added to adjust direction, and the ratio of the previous moment weights to those of the entire network is adjusted by momentum factors λ and ξ as shown in equation (15). After the introduction of the momentum factor, the influence of the

Figure 7 Basic structure of closed-loop control system of robot based on neural network

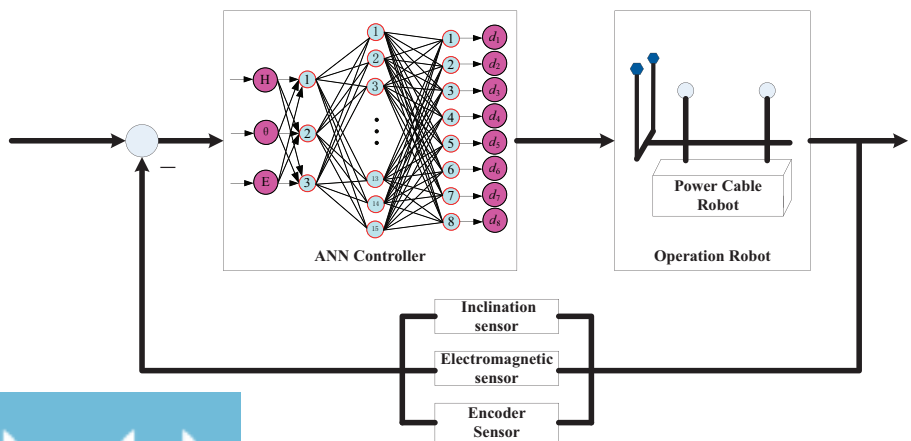

last change of weight of the network is transmitted through it. When ξ is zero, the weight change is adjusted only by gradient descent, which is the standard BP algorithm. When ξ is one, the new weight change of the network is set as the last weight change and the changed part produced by the gradient method can be ignored. In this way, adding the momentum term directs the adjustment of weights to the average at the bottom of the error surface, which helps the network jump out of the local minimum error surface and speed-up network convergence.

4.3 Time complexity and convergence analysis of BP algorithm

The time complexity of the algorithm is a function of the number of inputs n. This means that the basic number of operands used for the task when the algorithm completes the corresponding calculation is n, and can also intuitively be used to determine the performance of the method and its convergence speed. Therefore, the time complexity of the algorithm can be approximated as equation (16), wherein Max_Iteration is the maximum number of training sessions on the network:

$$O(\text{Max\_Iteration}) \tag{16}$$

Regarding the robot's general dynamic model and the object of operation, if the proper control torque is used, the dynamic error equation can be obtained as equation (17), wherein the parameters are defined as above:

$$M_i\ddot{e} + K_v\dot{e} + K_p e = 0 \tag{17}$$

The stability of the control system is a prerequisite for its normal operation. The stability of equation (17) is discussed below. The control system tends to be stable under the influence of wind load and a strong electric field. The Lyapunov function can be constructed as equation (18) and solved to derive equation (19). Combining it with equation (17), equation (20) can be obtained:

$$V = \frac{1}{2}\dot{X}_i^T M_i \dot{X}_i + \frac{1}{2}e^T K_p e \tag{18}$$

$$\dot{V} = \frac{1}{2}\dot{X}_i^T \dot{M}_i \dot{X}_i + \dot{X}_i^T M_i X_i - e^T K_p \dot{X}_i \tag{19}$$

$$\dot{V} = -\dot{X}_i^T K_v \dot{X}_i \le 0 \tag{20}$$

According to Lyapunov theory, the appropriate controlled torque can ensure tracking of the motion of the robot's joint from an arbitrary initial posture to the desired posture, with the motion tracking error converging to zero. It can also ensure the global asymptotic stability of the motion control system for the mechanical arm. Therefore, the system can be kept stable using the BP algorithm control.

5. Simulation and field operation

5.1 Simulation

To verify the validity of the improved BP neural network-based robot posture control method under typical operation conditions, a simulation was carried out with the manipulator 2 used for motion posture control. In the simulation, 1,000 samples were selected to train the BP neural network offline. According to the designed network structure and parameters, the initial learning rate was 0.045 and the adaptive adjustment strategy was adopted. The momentum factor was λ = 0.4, ξ = 0.6, the expected training error was 10^{-3}, and the maximum number of training steps was set to 1,000. In the above conditions, the training results of the standard BP algorithm and improved BP algorithm are shown in Figure 8. They show that under the same conditions, the standard BP algorithm converged to the given error after 49 training iterations while the improved BP algorithm converged after 33 iterations. Therefore, from the perspective of convergence speed, the improved algorithm had better control performance, and better satisfied the requirements of real-time control and stability of the robot on a high-voltage power cable line.

The curves of the wind load swing angle before and after neural network control were measured by an inclination sensor on the robot as shown in Figure 9. When the conductor slope was 12°, the maximum range of the wind bias deviation angle of the robot under the action of wind load controlled by the conventional PID algorithm can reach 9.5° to 14°. The range of the wind declination angle was thus clearly reduced by using neural network control. Moreover, the stabilization time of the robot was reduced. Therefore, the neural network controller can maintain the robust stabilization of the system. Furthermore, the results for the flexible sag and the robot's spatial field strength are shown in Figure 10. They show that the neural network controller can compensate for the effect of sag on the robot's posture. Updating its posture can help the robot choose a better operation trajectory planning path to avoid the influence of strong electromagnetic fields on its motion. Therefore, the simulation results verify the effectiveness of the proposed algorithm.

5.2 Field operation experiment

To further test the application to engineering problems of the neural network method for posture control of the robot under three typical operation conditions, bolt tightening of the tension clamp drainage plate was carried out by a robot in the right phase A of tower No. 003 on the 220-kV WangPei I line in the State Grid Hunan Electric Power Company. The tower type was SDN31-18, the conductor type was LGB20A-95/55, the insulator type was XP-7, and the number of insulators was 13. The effect and key process of the joint coordinated linkage of the dual manipulator to capture and locate the bolts and nuts from the initial posture to the ideal posture are shown in Figure 11. When the center line of the double manipulator sleeve was aligned with that of the bolt's head and nut, the edges of the sleeve and the nut could be aligned by rotating the bolt-tightening motor using a visual processing controller. Following the above two actions, the joint with bolts and nuts was subjected to the vertical movement of the dual manipulators to complete the robot's bolt-tightening operation. In the operation, the robot could compensate for the influence of flexible conductor sag, wind bias angle, and spatial field intensity on its motion posture by moving its joint. In the entire field operation experiment, the robot's operation arm entered the operation state in the initial state, and clamped the bolt head and nut with both manipulators. The robot's manipulator joints moved smoothly and continuously under disturbance due to wind load and strong electromagnetic interference. The manipulator located the key position accurately and successfully completed the bolt-tightening task.

Figure 8 Convergence curve of BP network

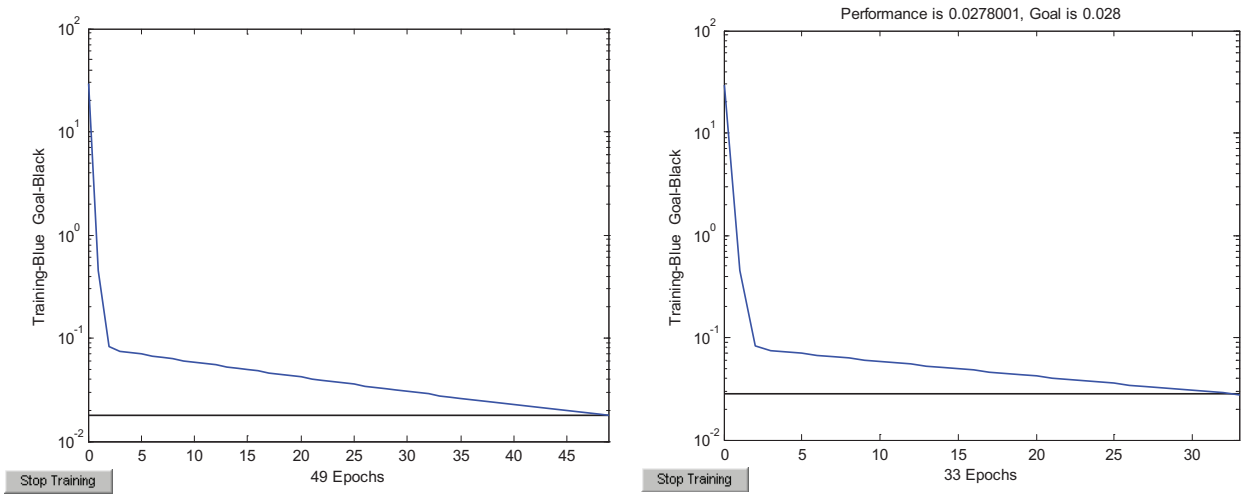

Notes: (a) Convergence curve of standard BP algorithm; (b) convergence curve of improved BP algorithm

Figure 9 Simulation curve of swing angle due to wind load

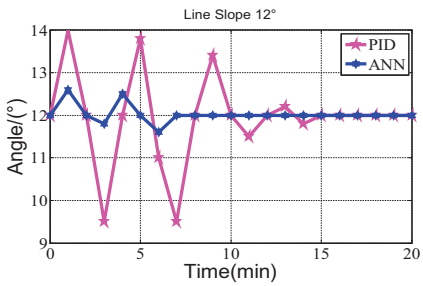

Figure 10 Curves of flexible environmental and electromagnetic field simulation

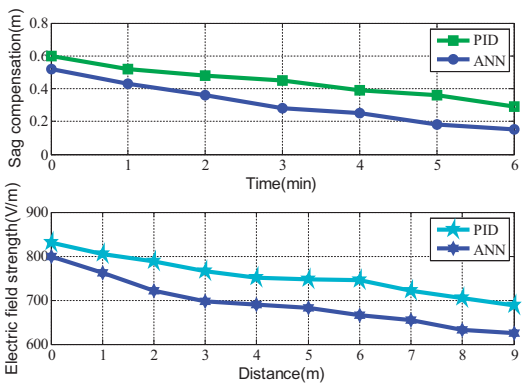

Figure 11 Field operation experiment

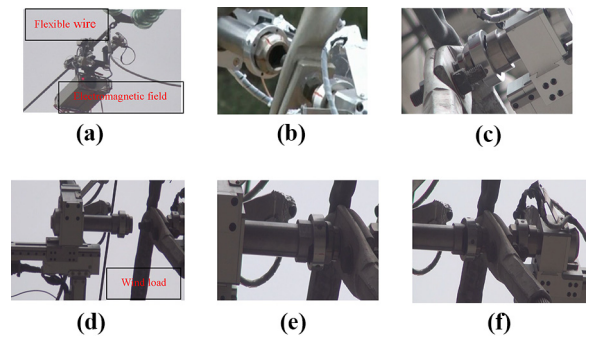

Notes: (a) Robot online; (b) locating bolt; (c) fixing bolt head; (d) locating nut; (e) docking with nut; (f) bolt-tightening operation

6. Conclusions and future works

6.1 Conclusions

- A multi-layer control architecture suitable for smart grid platform maintenance was proposed here, and a robot control system platform for network operation and maintenance management was constructed. Human–machine environmental coordination and integration, and an intelligent power system management platform can thus be implemented that significantly improves the intelligence of power system management.
- Mathematical models of the robot under three typical operation conditions of a flexible conductor, wind load and strong electromagnetic field were established, and the mapping relationship between environmental parameters and the robot's operation conditions was given. Through the nonlinear approximation characteristics of a BP network, the control variables of the robot's joints were obtained, and the influence of extreme power environments on its robot posture was compensated for.
- The simulation results of MATLAB show that the control algorithm can effectively restrain the influence of uncertain factors such as flexible environment, wind load and strong electromagnetic field on the robot posture. It satisfied the design requirements of fast response, high tracking accuracy and sound stability of the control

system. Field operation experiment further verifies the engineering practicability of the algorithm.

6.2 Future works

For robot manipulator posture control in power line environments, the structural parameters, internal and external disturbances and uncertainties require further research, and a theoretical model of the general posture error for different line environments should also be developed. The posture error self-compensation control strategy in this complex and variable environment would benefit from further study so that it can be applied to online monitoring for different operational tasks.

References

Banthia, V., Maddahi, Y., Balakrishnan, S. and Sepehri, N. (2014), "Haptic-enabled teleoperation of base-excited hydraulic manipulators applied to live-line maintenance", *Intelligent Robots and Systems (IROS 2014), 2014 IEEE/RSJ International Conference on. IEEE*, pp. 1222-1229.

Buehringer, M., Berchtold, J., Buchel, M., Dold, C., Bütikofer, M., Feuerstein, M. and Siegwart, R. (2010), "Cable-crawler-robot for the inspection of high-voltage power lines that can passively roll over mast tops", *Industrial Robot: An International Journal*, Vol. 37 No. 3, pp. 256-262.

Cuong, P.V. and Wang, Y.N. (2015), "Adaptive trajectory tracking neural network control with robust compensator for robot manipulators", *Neural Computing and Applications*, Vol. 27 No. 2, pp. 525-536.

Hong, Z., Wu, G., Wang, W. and Hu, P. (2016), "Posture detection and operation optimization of inspection robot under wind load", Vol. 54 No. 12, pp. 197-200.

Isaramongkolrak, A., Kerdpradub, P. and Wungwattana, K. (2014), "Comparative study for the installation of overhead ground wire affecting the electric field of high voltage transmission lines", *2014 International Conference on. IEEE*, pp. 1-7.

Kim, Y.H., Lewis, F.L. and Dawson, D.M. (2000), "Intelligent optimal control of robotic manipulators using neural networks", *Automatica*, Vol. 36 No. 9, pp. 1355-1364.

Korayem, M.H., Rahimi, H.N. and Nikoobin, A. (2012), "Mathematical modeling and trajectory planning of mobile manipulators with flexible links and joints", *Applied Mathematical Modelling*, Vol. 36 No. 36, pp. 3229-3244.

Lai, J., Lu, X., Wang, F., Dehghanian, P. and Tang, R. (2019), "Broadcast gossip algorithms for distributed peer-to-peer control in AC microgrids", *IEEE Transactions on Industrial Applications*, Vol. 55 No. 3, pp. 2241-2251.

Liu, Y.C., Liu, S.Y. and Wang, N. (2016), "Fully-tuned fuzzy neural network based robust adaptive tracking control of unmanned underwater vehicle with thruster dynamics", *Neurocomputing*, Vol. 196, pp. 1-13.

Montambault, S., Pouliot, N. and Lepage, M. (2012), "On the latest field deployments of LineScout technology on live transmission networks", *2nd International Conference on Applied Robotics for the Power Industry (CARPI)*, pp. 126-127.

Nandhakumar, S., Muthukumaran, V., Prakash, K.S. and Shunmughanaathan, V.K. (2013), "Position control of industrial robotic manipulator using variable structure control system with single term haar wavelet series method", *Journal of Vibration & Control*, Vol. 21 No. 12, pp. 211-225.

Pouliot, N., Mussard, D. and Montambault, S. (2012), "Localization and archiving of inspection data collected on power lines using LineScout technology", *Applied Robotics for the Power Industry (CARPI)*, pp. 197-202.

Pouliot, N., Richard, P.L. and Montambault, S. (2015), "LineScout technology opens the way to robotic inspection and maintenance of high-voltage power lines", *IEEE Power and Energy Technology Systems Journal*, Vol. 2 No. 1, pp. 1-11.

Ramirez, D., Ma, Y.B. and Bedir, S. (2014), "Introduction of a LIDAR-based obstacle detection system on the LineScout power line robot", *Journal of Endourology*, Vol. 28 No. 3, pp. 330-334.

Singh, J., Gandhi, K., Kapoor, M. and Dwivedi, A. (2013), "New approaches for live wire maintenance of transmission lines", *MIT International Journal of Electrical and Instrumentation Engineering*, Vol. 3 No. 2, pp. 67-71.

Sun, C., He, W. and Hong, J. (2016), "Neural network control of a flexible robotic manipulator using the lumped spring-mass model", *IEEE Transactions on Systems, Man, and Cybernetics: Systems*, Vol. 47 No. 8, pp. 1863-1874.

Sun, C., Zhao, M. and Wang, H. (2010), "Optimization of structural parameters of obstacle inspection robot under wind load", *Journal of Mechanical Engineering*, Vol. 46 No. 07, pp. 16-21.

Wang, J., Wang, Y., Peng, X., Li, X., Xu, X. and Mao, X. (2014), "Induced voltage of overhead ground wires in 50 0-kV single-circuit transmission lines", *IEEE Transactions on Power Delivery*, Vol. 29 No. 3, pp. 1054-1062.

Wang, X., Yu, Z. and He, J. (2014), "Breakdown process experiments of 110–500 KV insulator strings under short tail lingtning impulse", *IEEE Transactions on Power Delivery*, Vol. 5 No. 29, pp. 2394-2401.

Wu, X., Zhang, H. and Karady, G.G. (2017), "Transient analysis of inductive induced voltage between power line and nearby pipe line", *International Journal of Electrical Power & Energy Systems*, Vol. 84, pp. 47-54.

Xiao, X., Wu, G., Du, E., *et al.* (2005), "Dynamic simulation and experimental study of inspection robot for high-voltage transmission-line", *Journal of Central South University of Technology*, Vol. 12 No. 6, pp. 726-731.

Xiao, X., Wu, G., Du, E. and Li, S. (2008), "Impacts of flexible obstructive working environment on dynamic performances of inspection robot for power transmission line", *Journal of Central South University of Technology*, Vol. 15 No. 6, pp. 869-876.

Corresponding authors

Wei Jiang can be contacted at: jiangwei2017@wtu.edu.cn and **Hong Jun Li** can be contacted at: lihongjun@wtu.edu.cn